Journal of Nanophotonics

SPIEDigitalLibrary.org/jnp

Reflectivity enhanced two-dimensional dielectric particle array monolayer diffraction

Alexander Tikhonov
Nikolay Kornienko
Jian-Tao Zhang
Luling Wang
Sanford A. Asher

Reflectivity enhanced two-dimensional dielectric particle array monolayer diffraction

Alexander Tikhonov, Nikolay Kornienko, Jian-Tao Zhang, Luling Wang, and Sanford A. Asher
University of Pittsburgh, Department of Chemistry, Pittsburgh, Pennsylvania 15260
asher@pitt.edu

Abstract. Very high diffraction efficiencies (>80%) were observed from two-dimensional (2-D) photonic crystals made of monolayers of ~490 nm diameter dielectric polystyrene spheres arranged in a 2-D hexagonal lattice on top of a liquid mercury surface. These almost close packed 2-D polystyrene particle arrays were prepared by a self-assembly spreading method that utilizes solvent evaporation from the mercury surface. Two-dimensional arrays transferred onto a dielectric glass substrate placed on top of metal mirrors show diffraction efficiencies of over 30%, which is 6- to 8-fold larger than those of the same 2-D monolayers in the absence of mirrors. A simple single particle scattering model with refraction explains the high diffraction efficiencies in terms of reflection of the high intensity forward diffraction. © *2012 Society of Photo-Optical Instrumentation Engineers (SPIE).* [DOI: 10.1117/1.JNP.6.063509]

Keywords: diffraction; photonics; reflectance; photonic crystals; sensing.

Paper 12012 received Feb. 10, 2012; revised manuscript received Apr. 5, 2012; accepted for publication Apr. 5, 2012; published online Jun. 8, 2012.

1 Introduction

Two-dimensional (2-D) photonic crystals (PC) are of great interest owing to their potential applications in areas such as chemical sensing,[1–3] colloidal lithography,[4] and waveguiding.[5] The 2-D array PC is a 2-D diffraction grating that diffracts light into various Bragg diffraction orders. The diffracted beams either propagate outside the 2-D array PC[6,7] or propagate within the 2-D array PC in guided modes.[2,3,5,8–10]

The diffraction is relatively weak for low dielectric contrast 2-D array PCs. For example, 2-D array PCs of polystyrene particles in air back diffract 1% to 10% of the incident light, depending on the colloidal particle diameter.[11,12] The diffraction efficiency of dielectric 2-D PC generally increases with the magnitude of the 2-D PC dielectric constant modulation.[11–13] Very large diffraction efficiencies can be achieved from metallic 2-D array PC and/or by stacking dielectric 2-D layers to form strongly diffracting three-dimensional (3-D) PC.[1,14]

Maximizing the diffraction efficiency from a dielectric 2-D array PC is important for many applications. Although the transmission and specular reflection properties of 2-D array PCs relative to the excitation of the guided modes were previously examined (for example, Refs. 2, 3, 5, and 8–10), we are not aware of any quantitative measurements of 2-D array diffraction other than the zero order diffraction associated with transmission and reflection.

Here we measure the diffraction of a monolayer of polystyrene colloids that self-assemble into a 2-D hexagonal lattice on either dielectric or planar reflective substrates. We observe efficiencies of back-diffraction into a single diffraction order as high as 80% on a mercury surface and 30% from a 2-D hexagonal monolayer of polystyrene spheres arranged on a glass slide on top of a front surface aluminum mirror. The back diffraction intensity is 6- to 8-fold smaller in the absence of the mirror. We also find that the dielectric 2-D array first order diffracted beam on the forward transmission beam side (TS) is much more intense than diffracted beam on the backward incident beam side (IS). Placing the 2-D array PC on top of a mirror combines all diffracted beams, giving rise to a very strong diffraction, easily visible by eye.

0091-3286/2012/$25.00 © 2012 SPIE

The fact that the TS diffraction is much stronger than the IS diffraction is surprising from the point of view of the single sphere scattering approximation[15–17] since the scattering at the forward TS diffraction experimental angle of ~105 deg should give less single sphere scattering than in the backward IS direction. The simple modification of a single sphere scattering phenomenon to take into account refraction by the effective 2-D array refractive index medium can explain our observations.

2 Experimental

We utilized 489 ± 11 nm diameter highly charged polystyrene particles synthesized by emulsifier free emulsion polymerization.[18] The 2-D array PC was fabricated on a liquid mercury surface by self-assembly of these particles to form a 2-D monolayer [scanning electron microscope (SEM), Fig. 1].

We prepared a spreading solution containing 300 μL of a 14.4% weight fraction of colloidal particles in deionized water that was mixed with 200 μL of 1-propanol as a dispersing agent, 50 μL of hydroxyethylmethacrylate (HEMA), 20 μL of a 20 vol. % solution of the photoinitiator diethoxyacetophenone in 1-propanol, and 1 mg of the cross-linker bisacrylamide.

We gently layered 6.5 μL of the solution onto a clean mercury surface where it rapidly spread and formed an almost close packed polycrystalline 2-D colloidal crystal monolayer. The volume of solution added was designed to entirely coat the mercury surface with a close packed array of particles.

We then placed a vinyl group functionalized thin plastic sheet on top of the assembled array. This plastic sheet is manufactured by Bio-Rad Laboratories as a 65 mm × 125 mm × 100 μm gel support film. The 2-D monolayer was covalently attached to the plastic sheet by ultraviolet (UV) light polymerization of the HEMA surrounding the particle array. The 2-D array attached to the plastic sheet was then easily lifted from the mercury surface.

The SEM images in Fig. 1 show that the polystyrene particle array protrudes from the plastic sheet, indicating that the HEMA liquid layer coats and then polymerizes onto the plastic sheet surface. We calculate a poly-HEMA thickness of ~320 nm from the SEM measured apparent diameter of the spheres. This thickness is close to that expected from the amount of HEMA in the spreading solution.

We also attached the arrays to 25 mm × 75 mm × 1 mm glass microscope slides by a similar polymerization. Although the attachment of the array to the glass was not as strong as to the plastic sheet, with care we can completely lift the array attached to the microscope slide from the mercury surface.

Figure 1 shows SEM images of typically prepared 2-D monolayers on the plastic sheets. The 2-D monolayer is polycrystalline with almost close packed hexagonal ordering with ~10 to 15 μm length domains. The nearest neighbor particle spacing is calculated to be ~535 nm, slightly longer than the 489 ± 11 nm particle diameter.

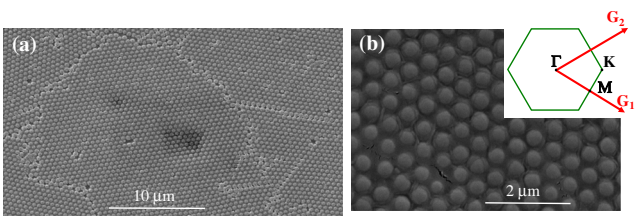

Fig. 1 SEM images of 2-D photonic crystals on a plastic sheet. (a) Polycrystalline 2-D particle array shows randomly oriented 10 to 15 μm domains. (b) The polymerized monolayer is an almost close-packed hexagonal array of 489 ± 11 nm diameter polystyrene particles with a nearest neighbor spacing of 535 nm. The inset shows the 2-D reciprocal lattice and the 2-D Brillouin zones with the Γ *K M* high symmetry points and the reciprocal lattice vectors $\vec{G}_1$ and $\vec{G}_2$.

3 Results and Discussion

We measured the angular dependence of the diffraction efficiency from the 2-D array PC by using a 532 nm laser beam with a diameter of ~1 mm, that is much larger than the individual hexagonal 2-D crystal domain size.

Figure 2(a) shows that for an incident angle of ~20 deg from the normal, numerous randomly oriented domains diffract light into two Debye diffraction rings. The intensity of the back diffracted ring on the IS is much less than that of the forward diffracted ring on the TS.

Figure 2(b) shows the calculated diffraction pattern for a 532 nm beam incident at 20 deg from the normal to a 2-D PC, that has a nearest neighbor spacing of 535 nm. We calculate the angular dependence of the 2-D diffracted beams from 300 different equally angularly spaced orientations of the 2-D array domains. The expected diffraction pattern consists of the zero diffraction order specular reflection and transmission beams, and the two first order diffraction beams that form the two Debye diffraction rings. These two Debye rings are situated symmetrically about the 2-D array PC plane with one on the IS of the array, while the other ring occurs on the TS of the array, as illustrated in Fig. 2(b).

The 2-D diffracted beam wavevectors fulfill the kinematic theory 2-D diffraction condition:

$$\vec{k}_{sc}^{\parallel} = \vec{k}_{in}^{\parallel} + \vec{G}, \tag{1}$$

where $\vec{k}_{in}^{\parallel}$ and $\vec{k}_{sc}^{\parallel}$ are the projections of the incident and diffracted light reciprocal wavevectors into the 2-D crystal plane, and $\vec{G}$ is any 2-D array reciprocal lattice vector. Figure 2(c) shows the 2-D reciprocal space plane that lies in the 2-D array PC plane that contains the 2-D array reciprocal lattice vectors $\vec{G}$ and vectors $\vec{k}_{in}^{\parallel}$ and $\vec{k}_{sc}^{\parallel}$.

In Fig. 2(c) the reciprocal lattice vectors $\vec{G}$ for all possible randomly oriented 2-D array crystal domains originate from the center of the red circle, P and end on its circumference.

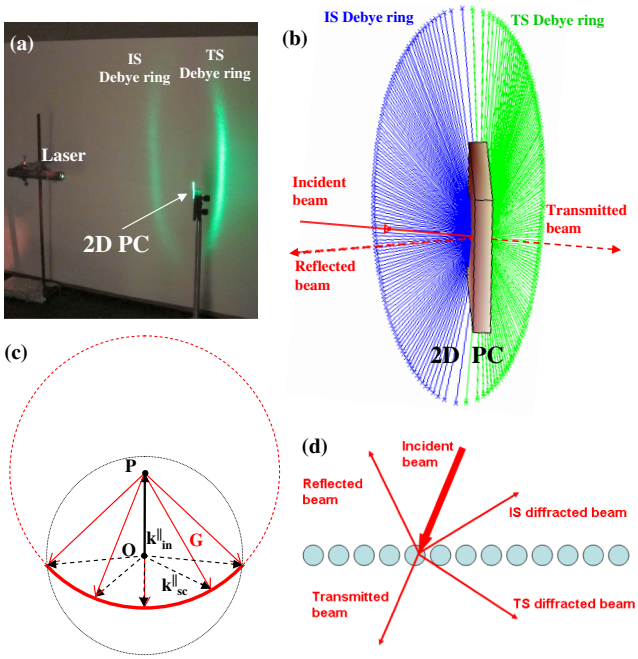

Fig. 2 (a) Photograph of 532 nm light diffraction from a 489 nm diameter polystyrene sphere 2-D array PC with a nearest neighbor spacing of 535 nm on a plastic sheet shows both the TS and IS Debye diffraction rings. The light is incident at 20 deg from the normal. (b) Calculated polycrystal 2-D array PC diffraction pattern for conditions above. (c) Reciprocal space for 2-D array polycrystal diffraction. Reciprocal 2-D lattice vectors $\vec{G}$ are shown as red arrows. The set of possible 2-D crystal domain orientation reciprocal lattice vectors $\vec{G}$ trace the red circle centered at *P*. The 2-D diffraction directions can be determined from $\vec{k}_{sc}^{\parallel} = \vec{k}_{in}^{\parallel} + \vec{G}$ and $|\vec{k}_{sc}^{\parallel}| \leq k$. Therefore, all allowed $\vec{k}_{sc}^{\parallel}$ indicated by the dashed arrows originate at *O* and end along the bold red arc. (d) Diagram illustrating the diffracted beams in our experimental geometry.

The projection of the incident light wavevector into the 2-D array plane is the light incident in-plane wavevector $\vec{k}_{\text{in}}^{\parallel} = \vec{OP}$. Its length depends upon its angle of incidence. In order to satisfy Eq. (1) the scattered vectors $\vec{k}_{\text{sc}}^{\parallel}$ must originate at point O and end on the red circle circumference. Since the projection $\vec{k}_{\text{sc}}^{\parallel}$ cannot be larger than $k = |\vec{k}_{\text{sc}}| = |\vec{k}_{\text{in}}|$, the allowed $\vec{k}_{\text{sc}}^{\parallel}$ must lie within the black circle with origin O and radius k. Therefore a Debye diffraction ring will be formed by all diffracted beams with $\vec{k}_{\text{sc}}^{\parallel}$ starting at O and ending on the bold red arc as defined by the black dashed arrows. The resulting Debye ring diffraction pattern is formed by these scattered $\vec{k}_{\text{sc}}$. The light from the Debye rings illuminate two arcs along the observation plane as observed in Fig. 2(a).

Figure 3(a) shows photographs of the diffracted colors from a white light beam incident at 30 deg from the normal onto a 2-D array spread on a mercury surface (left) and on a plastic sheet (right). The photographs were taken at the different viewing angles shown. The diffracted light wavelength decreases as the viewing angle moves towards the array normal, as expected for 2-D diffraction. The brightness of the 2-D diffraction pattern for the 2-D array PC on the mercury is obviously much higher than from the array on a plastic sheet.

Figure 3(b) shows for 532 nm light the measured and calculated dependence of the diffraction angle in the plane of the 2-D array PC normal and the ΓM symmetry axis [Fig. 1(b)] of the 2-D Brillouin zone of a hexagonal lattice on the incident angle. This measurement is for diffraction from the 2-D array attached to a plastic sheet. The diffraction occurs from domains oriented with their ΓM direction within this plane. Both $\vec{k}_{\text{in}}^{\parallel}$ and $\vec{k}_{\text{sc}}^{\parallel}$ are parallel to the reciprocal lattice vector $\vec{G}$. The 2-D diffraction condition is $|\vec{k}_{\text{sc}}^{\parallel}| + |\vec{k}_{\text{in}}^{\parallel}| = |\vec{G}|$ which gives $m\lambda = d\frac{\sqrt{3}}{2}[\sin(\alpha_{\text{dif}}) + \sin(\alpha_{in})]$, where d is the spacing between nearest neighboring particles, m is the diffraction order, and α_{in}

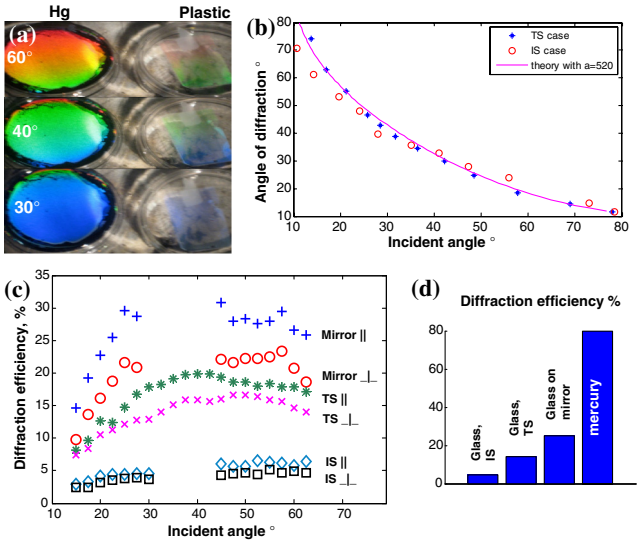

Fig. 3 (a) Photographs of diffraction colors for a 2-D array PC on a mercury surface (left) and on a plastic sheet (right) from incident white light at 30 deg from the normal. Top to bottom photographs are recorded at decreasing observation angles (60, 40, and 30 deg) showing the expected 2-D diffraction blue shift. (b) For 532 nm light the measured and calculated IS and TS diffraction beam angular dependence on the incident beam angle within the plane containing the incident, diffracted and ΓM direction for a 2-D array PC on a plastic sheet. Calculated dependence is for a nearest neighbor particle spacing of 520 nm. (c) Incident beam angular dependence of IS and TS diffraction efficiencies for 2-D array PC on a glass slide, and IS diffraction efficiency of the same 2-D array PC placed such that the glass contacts a front surface aluminum mirror for parallel and perpendicularly polarized 532 nm incident light. (d) 25 deg incident angle parallel polarization IS and TS diffraction efficiencies from 2-D array PC on glass slide. IS diffraction efficiencies from the same 2-D array PC on glass slide placed such that the glass side lies on a front surface aluminum mirror, and from a 2-D array self assembled on a mercury in the absence of a plastic sheet or glass slide.

and α_{dif} are the incident and diffracted angles from the normal. The measured diffraction angles for both the TS and IS (relative to the 2-D PC plane) diffracted light agree well with those calculated for $d = 520$ nm [Fig. 3(b)].

Figure 3(c) shows the measured angular dependence of the diffraction efficiency of a 532 nm laser beam from the 2-D array PC attached to a glass microscope slide in the case that the diffracted beam lies in the same plane as the incident beam and the 2-D plane normal. The intensity diffracted into the Debye ring was estimated by measuring the intensity diffracted into a small area of the Debye ring and then dividing this intensity by the relative fraction compared to the total ring. The intensity per unit area measured from different regions of the Debye ring is relatively constant, varying by <20%.

For a 532 nm parallel polarized beam incident at 25 deg from the normal to the 2-D array PC on the glass slide we measured a diffraction efficiency of 4.5% for the IS and 15% for the TS Debye rings [Fig. 3(d)]. In contrast, we measured a 30% diffraction efficiency (that is larger than the sum of the TS and IS diffracted intensities in the absence of the mirror) from the same 2-D array PC on the glass slide when we placed its glass side on a front surface aluminum mirror. A 2-D array PC self assembled on the mercury shows an even larger diffraction efficiency of ~80% at the same incidence angle.

This increased IS diffraction efficiency from the 2-D array PC spaced from the Al mirror by 1 mm glass thickness can be easily rationalized by using the single particle scattering approximation for dielectric spheres on a dielectric substrate,[15–17] or for dielectric spheres spaced at least ~5 wavelengths away from a metal surface.[17]

In this model the diffraction of the 2-D sphere array spaced by the glass slide from the metal mirror results from a combination of diffraction and reflection processes. Figure 4 shows that light incident on the 2-D array PC diffracts into IS and TS beams D1 and D2. The TS diffracted beam D2 is then reflected by the mirror to form beam D2' which is parallel to D1. The incident light transmitted through the 2-D array PC is reflected by the mirror and diffracts from the 2-D array PC, resulting in the diffracted beam D3 that also propagates parallel to D1. The diffracted beam D4 is reflected forming D4' that also propagates parallel to D1. The total diffracted intensity is $D1 + D2' + D3 + D4'$. In contrast, for the 2-D PC on a glass slide we only observe diffracted beam D1. The increased diffraction intensity observed with the mirror results from the additional contribution of the TS diffraction. In our system TS diffraction is much larger than IS diffraction.

Our explanation, at the present time, for the high observed diffraction efficiency from the 2-D arrays on reflective surfaces sums these 4 beams at the intensity level, ignoring the possibility of interference between the different beams. We neglect this possibility because we expect that the mercury surface, as well as the other reflective surfaces are rough and the presence of dust may cause variations of the spacing of the array from the reflective surface. Future studies will examine the possibility of interference phenomena.

The even larger diffraction efficiency from the 2-D array on mercury probably results from its better ordering. The decreased ordering of the 2-D array on glass occurs due to the manipulation involved in placing the glass slide on top of the array on mercury, polymerizing the array and lifting it from the mercury surface.

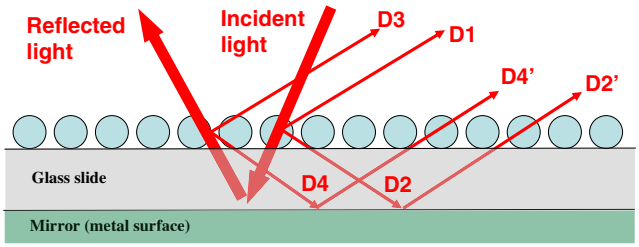

Fig. 4 Diffraction from a 2-D array PC separated by a layer of glass from a mirror. The incident light diffracts into IS and TS beams D1 and D2. Light transmitted through the 2-D PC is reflected by the mirror and then diffracted by the 2-D PC into its respective IS and TS beams D4' and D3. The total diffracted intensity in the IS direction is the sum of intensities $D1 + D2' + D3 + D4'$.

Figure 3(c) shows that for incident angles between 15 and 65 deg for the 2-D array PC on the glass slide the TS diffracted light intensity is 2 to 2.5 times larger than the IS diffracted light. The dominance of TS diffraction over the IS diffraction results from the Mie scattering of these spherical particles as shown by Fig. 5(a) that shows the Mie single sphere scattering diagram for a dielectric sphere of 490 nm diameter with a refractive index of 1.58 in an air-poly-HEMA medium with an estimated volume averaged refractive index of 1.26.

The Fig. 5(a) Mie scattering diagram for 532 nm light shows the dependence of scattered intensity on the scattering angle, where we plot the differential scattering cross section per unit solid angle. The Mie scattering is strongly asymmetric with forward scattering much stronger than backward scattering. The perpendicular polarized backward scattering intensity occurs as a single small lobe with a maximum in the exact backward scattering angle of 180 deg. The parallel polarized backward scattered intensity shows a more complex dependence on the scattering angle showing three lobes.

To relate the Fig. 5(a) single sphere angular dependent scattering efficiency to the angular dependence of the 2-D array diffraction efficiency, we must calculate the effective single sphere scattering angles ϕ_{IS} (ϕ_{TS}) between incident beam and the IS (TS) diffraction angles. These scattering angles are $\phi_{IS} = \alpha_{dif} - \alpha_{in}$ and $\phi_{TS} = 180° - \alpha_{dif} - \alpha_{in}$, where the incident and diffraction angles α_{in} and α_{dif} are defined relative to the 2-D PC normal, and are calculated by including Snell's law refraction for transmission of the incident beam from the air into the dielectric medium and transmission of the diffracted beam from the dielectric medium (consisting of the polystyrene particles in the thin poly-HEMA layer) to the air.

Figure 5(b) show the dependence of the IS and TS calculated scattering angles ϕ_{IS} and ϕ_{TS} on the incident angle. For incident angles between 15 to 65 deg the TS scattering angle ϕ_{TS} remains approximately constant at ~133 deg, and the corresponding single sphere differential scattering cross section is ~0.025 (~0.03) μm^2 for the perpendicular (parallel) polarization [red curve in Fig. 5(a)]. For the same range of incident angles 15 to 65 deg the IS scattering angle ϕ_{IS} varies between −25 and 25 deg, and the corresponding differential scattering cross section lies between ~0.002 to ~0.003 μm^2 for both perpendicular and parallel polarizations.

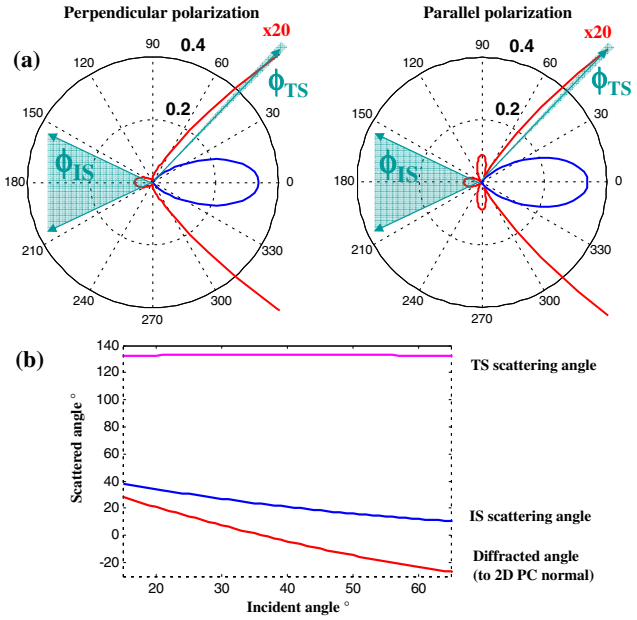

Fig. 5 (a) 532 nm light scattering Mie diagrams for a 490 nm diameter sphere of refractive index of 1.58 in a medium of refractive index 1.26 show differential scattering cross sections (μm^2 str^{-1}). Left is for perpendicular polarized light. Right is for parallel polarized light. Range of TS and IS single sphere scattering angles corresponding to a 15 to 65 deg range of incident angles that is enclosed by the blue triangles. (b) TS and IS calculated single sphere scattering angles ϕ_{TS} and ϕ_{IS} dependencies on the incident angle, defined relative to the 2-D array PC normal.

The large increased single sphere scattering power in the TS direction relative to the IS direction explains that the observed data in Fig. 3(b) results from the much stronger Mie forward scattering efficiency.

It is essential to include Snells law refraction to explain our experimental observations. Without taking into account refraction the TS scattering angle is ~105 deg and the IS scattering angle varies between −20 and 20 deg. For these scattering angles, the single sphere scattering in TS direction would be less then in the IS directions (Fig. 5). Snell's law refraction accounts for the fact that the local field incident and diffracted fields from the sphere array are a combination of the incident electric field and the scattered fields from all other spheres. We approximate the contribution of the other spheres by invoking an effective medium approximation[19] and calculating the directions of the local incident and local scattered fields as if individual spheres were embedded in a homogeneous layer with an effective volume averaged refractive index.

However the inclusion of refraction is not trivially obvious since the 2-D diffraction condition is independent of the refractive index of the 2-D array particles and monolayer medium.[20] The effect of the refractive index on refraction at the monolayer interface cancels the impact of the refractive index on the wavelength of light. For example, in the Littrow configuration with $\vec{k}_{\text{in}} = -\vec{k}_{\text{sc}}$ the 2-D Bragg diffraction relation does not depend on refractive index: $m\lambda_0 = 3\frac{1}{2}d \sin\theta$, where m is the diffraction order, λ_0 is the diffracted wavelength (in vacuum), d is the 2-D particle spacing, and θ is the angle relative to the normal to the 2-D array. For a fixed 2-D array spacing changing the monolayer refractive index does not change the diffraction condition but changes the relative diffracted intensity ratio between the IS and TS diffracted beams.

4 Summary

We report the first measurements of the light diffraction efficiency from a dielectric 2-D array PC on dielectric and metal substrates. We prepared almost closed packed 2-D polystyrene particle arrays by solvent evaporation of self assembling monolayers on mercury surfaces. The 532 nm light diffraction efficiency from a 2-D array PC on a glass slide in the TS direction was measured to be 3- to 4-fold larger then in the IS direction. This difference is due to larger Mie forward scattering intensities of single sphere scattering. The observed scattered diffraction efficiency is extraordinarily high, reaching 80% for a 2-D array PC on a mercury surface. The observed diffraction efficiency is only 30% for a 2-D array PC on a glass slide placed on a front surface aluminum mirror.

These high diffraction efficiencies of monolayer arrays of polystyrene spheres enable their use as visually evident chemical sensing materials.[21]

Acknowledgments

The authors are grateful for the financial support from HDTRA (Grant No. 1-10-1-0044). All authors of the paper contributed significantly to the work reported in this manuscript.

References

1. X. Yu et al., "High quality factor metallodielectric hybrid plasmonic–photonic crystals," *Adv. Funct. Mater.* **20**(12), 1910–1916 (2010), http://dx.doi.org/10.1002/adfm.v20:12.
2. L. Shi et al., "Guided-mode resonance photonic crystal slab sensors based on bead monolayer geometry," *Opt. Express* **16**(22), 17962–17971 (2008), http://dx.doi.org/10.1364/OE.16.017962.
3. J. Ge and Y. Yin, "Responsive photonic crystals," *Angew. Chem. Int. Ed.* **50**(7), 1492–1522 (2011), http://dx.doi.org/10.1002/anie.200907091.
4. J. Zhang et al., "Colloidal self-assembly meets nanofabrication: from two-dimensional colloidal crystals to nanostructure arrays," *Adv. Mater.* **22**(38), 4249–4269 (2010), http://dx.doi.org/10.1002/adma.201000755.

5. S. Fan and J. D. Joannopoulos, "Analysis of guided resonances in photonic crystal slabs," *Phys. Rev. B* **65**(23), 235112 (2002), http://dx.doi.org/10.1103/PhysRevB.65.235112.
6. G. von Freymanna et al., "Diffraction properties of two-dimensional photonic crystal," *Appl. Phys. Lett.* **83**(4), 614–616 (2003), http://dx.doi.org/10.1063/1.1596731.
7. G. Alagappan, X. W. Sun, and M. B. Yu, "Out-of-plane diffraction of a two-dimenisonal photonic crystal with finite dielectric modulation," *J. Opt. Soc. Am. A* **25**(5), 1098–1103 (2008), http://dx.doi.org/10.1364/JOSAA.25.001098.
8. Y. Kurokawa, H. Miyazaki, and Y. Jimba, "Light scattering from a monolayer of periodically arrayed dielectric spheres on dielectric substrates," *Phys. Rev. B* **65**(20), 201102 (2002), http://dx.doi.org/10.1103/PhysRevB.65.201102.
9. M. Inoue, "Enhancement of local field by a two-dimensional array of dielectric spheres placed on a substrate," *Phys. Rev. B* **36**(5), 2852–2862 (1987), http://dx.doi.org/10.1103/PhysRevB.36.2852.
10. K. Ohtaka et al., "Photonic band effects in a two-dimensional array of dielectric spheres in the millimeter-wave region," *Phys. Rev. B* **61**(8), 5267–5279 (2000), http://dx.doi.org/10.1103/PhysRevB.61.5267.
11. K. Busch et al., "Periodic nanostructures for photonics," *Phys. Rep.* **444**(3–6), 101–202 (2007), http://dx.doi.org/10.1016/j.physrep.2007.02.011.
12. A. Tikhonov, R. D. Coalson, and S. A. Asher, "Light diffraction from colloidal crystals with low dielectric constant modulation: simulations using single-scattering," *Phys. Rev. B* **77**(23), 235404 (2008), http://dx.doi.org/10.1103/PhysRevB.77.235404.
13. A. V. Baryshev et al., "Light diffraction from opal-based photonic crystals with growth-induced disorder: experiment and theory," *Phys. Rev. B* **73**(20), 205118 (2006), http://dx.doi.org/10.1103/PhysRevB.73.205118.
14. S. A. Asher et al., "Diffraction in crystalline colloidal-array photonic crystals," *Phys. Rev. E* **69**(6), 066619 (2004), http://dx.doi.org/10.1103/PhysRevE.69.066619.
15. M. A. Taubenblatt and T. K. Tran, "Calculation of light scattering from particles and structures on a surface by the coupled-dipole method," *J. Opt. Soc. Am. A* **10**(5), 912–919 (1993), http://dx.doi.org/10.1364/JOSAA.10.000912.
16. K. B. Nahm and W. L. Wolfe, "Light scattering models for spheres on a conducting plane: comparison with experiment," *Appl. Opt.* **26**(15), 2995–2999 (1987), http://dx.doi.org/10.1364/AO.26.002995.
17. B. R. Johnson, "Light scattering from a spherical particle on a conducting plane: I. normal incidence," *J. Opt. Soc. Am. A* **9**(8), 1341–1351 (1992), http://dx.doi.org/10.1364/JOSAA.9.001341.
18. C. E. Reese and S. A. Asher, "Emulsifier-free emulsion polymerization produces highly charged, monodisperse particles for near infrared photonic crystals" *J. Coll. Interf. Sci.* **248**(1), 41–46 (2002), http://dx.doi.org/10.1006/jcis.2001.8193.
19. M. Meier, A. Wokaun, and P. F. Liao, "Enhanced fields on rough surfaces: dipolar interactions among particles of sizes exceeding the Rayleigh limit," *J. Opt. Soc. Am. B* **2**(6), 931–949 (1985), http://dx.doi.org/10.1364/JOSAB.2.000931.
20. T. Kanai, T. Sawada, and K. Kitamura, "Optical determination of the lattice constants of colloidal crystals without use of the refractive index," *Langmuir* **19**(6), 1984–1986 (2003), http://dx.doi.org/10.1021/la0268855.
21. J. Zhang et al., "2-D array photonic crystal sensing motif," *Am. J. Chem. Soc.* **133**(24), 9152–9155 (2011), http://dx.doi.org/10.1021/ja201015c.

Alexander Tikhonov is recently moved to a position of a leading research scientist at Center for Energy Research at Nazarbayev University, Kazakhstan. He was a research assistant professor at the University of Pittsburgh, Pennsylvania. His recent research focuses in fabrication, characterization and applications of photonic colloidal crystals. He works in both theory and experiment in the fields of photonic properties of nanomaterials and molecular electronics.

Nikolay Kornienko received his BS in chemistry from the University of Pittsburgh and is currently a PhD student in the department of chemistry at the University of California, Berkeley. He is working in the research group of professor Peidong Yang on the synthesis of semiconductor nanowires and utilizing them for solar to fuel conversion. His research interests include fabrication and investigation of the properties of photonic crystals, synthesis and characterization of novel nanomaterials, and applications of semiconductors for photoelectrochemistry and photovoltaics.

Jian-Tao Zhang received his PhD from Wuhan University, China in 2005. He was a postdoc at IBN, A-Star, Singapore in 2006 and then an Alexander-von-Humboldt Fellow and a Carl-Zeiss Fellow in Jena University, Germany. He joined Asher's lab in University of Pittsburgh in 2010 and now is a research assistant professor. His research focuses on photonic crystal hydrogel materials for optical sensing applications, colloid nanoparticle self-assembly, and functional hybrid materials.

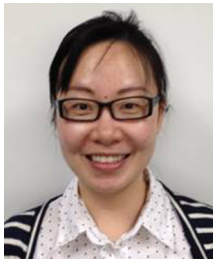

Luling Wang received her PhD in chemistry from University of Pittsburgh in 2012. She is currently a senior research chemist at Fujifilm Electronic Materials USA, Inc. Her research areas include photonic crystals, nanomaterials, polymers, colloid design and fabrication, deep UV filters, UV Raman explosive detection, and Raman spectroscopy. Her recent research is focused on developing chemical mechanical polishing slurries with different application goals.

Sanford A. Asher is distinguished professor of chemistry, University of Pittsburgh. His research develops new materials and spectroscopic techniques. His group developed UV resonance Raman spectroscopy (UVRR) as a technique for fundamental and applied structural and trace studies of molecules in complex matrices. They utilize UVRR to examine the first stages in protein folding and use UVRR for stand-off detection of explosive molecules. His group pioneered the development of new photonic crystal and chemical sensing devices from self-assembling colloidal particles coupled to smart hydrogel materials. He has authored more than 265 publications and 25 patents in the area of photonic crystals. Recent awards include: 2011 Charles Kaufman Award; 2008 SSP Pittsburgh Spectroscopy Award; 2007 Fellow of the Society of Applied Spectroscopy; 2005 Sigi Ziering Award; 2004 University of Missouri, Distinguished Alumni Award; 2002 ACS Pittsburgh Award; 2002 Ellis Lippincott Award; 1999 Bomen-Michelson Award, Coblentz Society, 2000 Pittsburgh Technology Council Enter Prize Award.